# Experimental study of a pilot-scale fin-and-tube phase change material storage

Giorgio Besagni*, Lorenzo Croci

Ricerca sul Sistema Energetico - RSE S.p.A., Power System Development Department, via Rubattino 54, 20134, Milan, Italy

* Corresponding author: Giorgio Besagni, giorgio.besagni@rse-web.it, Ricerca sul Sistema Energetico - RSE S.p.A., Power System Development Department, via Rubattino 54, 20134 Milan (Italy)

## Abstract

The large-scale deployment of solar-assisted systems in the residential sector relies on innovative thermal energy storage units. This paper contributes to the present-day discussion by proposing a pilot-scale phase change material storage, whose size has been selected to be coupled with solar-assisted heat pumps. The storage unit consists of a fin-and-tube heat exchanger placed within a tank: water is circulated on one side of the heat exchanger and, on the other side, commercial paraffin RT26 is employed. The storage system is operated considering two heat exchanger configurations (viz., parallel and series configurations) and implementing a broad set of boundary conditions, to test the storage unit under relevant operating conditions. To this end, a novel test rig with electrical resistances (to provide the heating load) and a heat pump (to provide the cooling load) has been designed and build. The results were commented in terms of global and local performances; it was found that the proposed storage, compared with a volume-equivalent water storage, is able to store 65 % higher thermal energy. In addition, the dataset obtained in this research is attractive to validate numerical codes of phase change material storage units.

**Keywords.** Phase change material; Thermal energy storage; Solar-assisted systems; Experimental study

# Nomenclature

## Acronyms

| | |
|---|---|
| PCM | Phase Change Material |
| RSE | Ricerca sul Sistema Energetico |
| SAHP | Solar-Assisted Heat Pump |

## Symbols

| | | |
|---|---|---|
| $c_p$ | Specific heat of water | [J/kg K] |
| $E_{th}$ | Charge/discharge energy | [Wh] |
| $E_{th,heating}$ | Energy stored during the charging phase in Eq. (2) | [Wh] |
| $\dot{m}$ | Mass flow rate | [kg/s] |
| $P_{el}$ | Power provided by the electrical resistances | [kW] |
| $\dot{Q}$ | Instantaneous power in Eq. (1) | [kW] |
| $Re$ | Reynolds number | [-] |
| $t$ | Temporal variable in Eq. (2) | [s] |
| $T_1$ | Temperature at location #1 inside the storage unit (Figure 2) | [°C] |
| $T_2$ | Temperature at location #2 inside the storage unit (Figure 2) | [°C] |
| $T_3$ | Temperature at location #3 inside the storage unit (Figure 2) | [°C] |
| $T_{average}$ | Average temperature inside the storage unit | [°C] |
| $T_{inlet}$ | Temperature at the inlet of the storage unit | [°C] |
| $T_{heating}$ | Temperature at the outlet of the storage unit at the end of phase#1 | [°C] |
| $T_{outlet}$ | Temperature at the outlet of the storage unit | [°C] |
| $T_{start}$ | Temperature of the storage unit at the beginning of the test | [°C] |
| $UA$ | Overall heat transfer coefficient | [W/k] |
| $\dot{V}$ | Volumetric flow rate | [$m^3$/h] |
| $\dot{V}_{heating}$ | Volumetric flow rate in the heating phase | [$m^3$/h] |
| $\dot{V}_{cooling}$ | Volumetric flow rate in the cooling phase | [$m^3$/h] |

## Greek symbols

| | | |
|---|---|---|
| $\varepsilon_{m,heating}$ | Mass energy density in the heating phase | [Wh/kg] |
| $\varepsilon_{V,heating}$ | Volume energy density in the heating phase | [Wh/$m^3$] |

# 1 Introduction

The decarbonisation of energy systems is a priority in the international research agenda and a matter of intense discussion among policy makers. In this framework, the so-called "*energy metabolism*" of a country is determined by the equilibrium between the supply-side and the demand-side at the "*household-scale*" (in the residential sector) and at the "*factory-scale*" (in the industrial sector). This paper focuses on the residential sector, which is responsible for a considerable share of the primary energy consumption of the different countries, as widely discussed by Brounen et al. [1]. In particular it accounts for approximately 50% of the total final energy consumption within the *EU28* region [2] and up to approximately 85% of the household final energy consumption [3]. Looking closer at the determinants of the energy consumption in the residential sector, thermal energy technologies and the end-used behavior determine the supply-side and the demand side, respectively. For this reason, the demand-side/supply-side equilibrium point is a function of technological and socio-demographic variables under geographical constrains (please refer to the statistical study proposed by Besagni and Borgarello [4]). The demand-side/supply-side equilibrium point is also time dependent on the daily and the seasonal time-scales and changing this relationship is of paramount importance within the demand-side managing perspective [5]. To obtain a feasible control of above-mentioned equilibrium, electrical/thermal energy storage technologies need to be deployed. For example, the use of thermal energy storages in the context of the demand management was discussed by Arteconi et al. [6], Allison et al. [7] and Nkwetta et al. [8]. Within this complex framework, this paper contributes to the present discussion regarding thermal energy storages for solar-assisted heat pumps, *SAHPs* (viz., a "*low-temperature*" application, requiring storage temperatures in the range of 20 - 30 °C). This topic is of paramount importance, as the deployment of *SAHPs* at the "*household-scale*" is widely recognized a preferential path towards "*low-carbon economies*". Unfortunately, the performances of *SAHPs* are highly related to the availability of the solar source and, thus, thermal energy storage should be deployed and carefully designed; in this respect, Buker and Riffat [9] proposed an interesting literature review. Recently the importance of thermal energy storage was demonstrated in the field study of Besagni et al. [10], who designed, built and tested a dual-source *SAHP*. They concluded that a mandatory step forward towards large-scale deployments of *SAHPs* is the development of innovative and economical viable, thermal storage units.

Recently, Zhang et al. [11] proposed a comprehensive literature survey where a fundamental classification of thermal energy storage units was given: (i) thermochemical storages and (ii) latent heat storages (viz., phase change materials,

*PCMs*). As stated above, the target of this paper concerns the residential sector, where *PCM* storages are of particular interest (i.e., for domestic how water production [12], integration with heat pumps and *SAHPs* [13], …), owing to their thermophysical properties and advantages (i.e., high energy storage density within a narrow temperature range) [14, 15]. Kenisarin [15] proposed a complete discussion regarding *PCMs* properties, whereas a Pereira da Cunha and Eames [16] discussed *PCMs* application for low- and medium-temperature applications, pointing out that the *PCM* selection depends on the operating range of temperatures. Out of the many practical examples and cases studied, Pereira da Cunha and Eames [17] studied a *PCM* storage for a multifunctional air-source heat pump and compared its performance with a conventional gas boiler, showing promising outcomes; Frazzica et al. [28] experimentally studied a hybrid sensible/latent storage system for domestic how water production. When designing pilot-scale[1] experimental facilities, the local phenomena should be taken into account and, within this perspective, Kabbara et al. [26] proposed an experimental study regarding a coil-in-tank PCM storage. They found that natural convection dominates the melting phase, whereas conduction dominates the solidification phase. Despite the promising characteristics of *PCM* materials, their utilization in thermal energy storages (and, in turn, the large-scale deployment of *PCM* storage units) is still limited because of a major shortcoming: the low thermal conductivity. Despite some heat transfer enhancement methods were proposed, a widely accepted solution is far from being achieved. Accordingly with Zhang et al. [11] the prevailing heat transfer enhancement methods are as follows: (i) finned tubes, (ii) *PCM*–graphite materials, (iii) micro/macro encapsulation, (iv) inclusion of metallic particles, (v) inclusion of *PCM* within a metal. Among the different methods, finned tubes have attracted a growing interest, especially as they allow the use of commercially available heat exchanges [21]. Medrano et al [18] proposed a comparative analysis of different storage units and concluded that the finned one results in high heat storage capacity and higher power output. Following a similar perspective, Frazzica et al. [30] experimentally compared a fin-and-tubes heat exchanger and a commercial asymmetric plate heat exchanger. Agyenim et al [19] observed that longitudinal or circular fins lead to an increase in the discharge efficiency equal to a 20% compared with a baseline case. Eslamnezhad and Rahimi [20] proposed a numerical study devoted to find the optimum fin arrangements to increase heat transfer in finned and tube PCM systems. Gasia et al. [27] experimentally studied the performance of different heat transfer enhancement techniques (i.e., metallic finds, inclusion of metals within the thermal storage,…) and suggested that metal finds provided the overall better outcomes. Acır and Canli [21] experimentally studied heat transfer enhancement in PCM systems, by

[1] "*pilot-scale*" refers to an experimental set-up, whose scale is suitable for an integration with an existing facility.

79 the use of fins and compared different systems layout in terms of efficiency and melting rate. Finned storage units, for
80 applications in the range of 70 – 90 °C, were designed and tested by Palomba et al. [22]. Based on the current state-of-
81 the-art, it is worth noting that pilot-scale experimental studies under controlled boundaries are rare, as discussed by
82 Dolado et al. [23], Peiró et al. [24] and Palomba et al. [22]. These studies pointed out the necessity of pilot-scale
83 experimental studies to clarify the storage behaviour under typical working conditions. In addition, such experimental
84 observations are of paramount importance to validate numerical codes [25].

85 Given the state-of-the-art, this paper contributes to the existing discussion regarding pilot-scale *PCM* storage units for
86 residential applications. In this perspective, this paper tackles this problem at hand: a novel pilot-scale phase change
87 materials storage for *SAHPs* (viz., storage temperatures in the range of 20 - 30 °C, accordingly with the outcomes of
88 Besagni et al. [10]) is designed and tested. In addition, a laboratory test rig has been designed and build, to study the
89 influence of the boundary conditions (e.g. flow rate, inlet/outlet temperatures, heating loads, …) on the local and
90 global performances of the storage unit. To the authors' best knowledge, this is one of the very few experimental
91 studies regarding pilot-scale *PCM* storage units for low-temperature applications. The remaining of the article is
92 organised as follows. Section 2 presents the experimental setup and methods; Section 3 presents the experimental
93 results and, finally, the concluding remarks are formulated in Section 4.

# 94 2 Experimental setup and methods

## 95 2.1 Test rig

96 Figure 1 displays the test rig developed within this research and build in a detached house (Milan, Latitude 45.47°,
97 Longitude 9.25); Figure 1 proposes an overview of the different system components, the measured variables and the
98 storage unit layout (further discussed in Section 2.2[2]); conversely, Table 1 lists the details of the system components
99 and instrumentation. The test rig aims testing the storage unit by imposing a realistic set of boundary conditions (e.g.
100 flow rate, inlet/outlet temperatures, heating loads, …). To this end, a reversible heat pump (component*#1* in Figure 1)
101 is used to impose cooling loads, by maintaining the "*buffer storage tank*" (component*#3* in Figure 1) at a set-point
102 temperature (equal to 15 °C), this acting as a heat sink. The "*buffer storage tank*" is connects to the *PCM* storage by an

[2] The storage unit was placed outside the detached house owing to internal regulation of our research centre (viz., parafine material is not allowed to be used inside buildings).

hydraulic circuit composed by a deviation valve (component*#4* in Figure 1) and a plate heat exchanger (component*#9* in Figure 1); in this circuit, a variable speed pump imposes the propylene-water-glycol mixture flow rate and two electrical resistances (component*#8* in Figure 1) impose the heating load ($P_{el}$). All pipes and system components were insulated to avoid thermal losses.

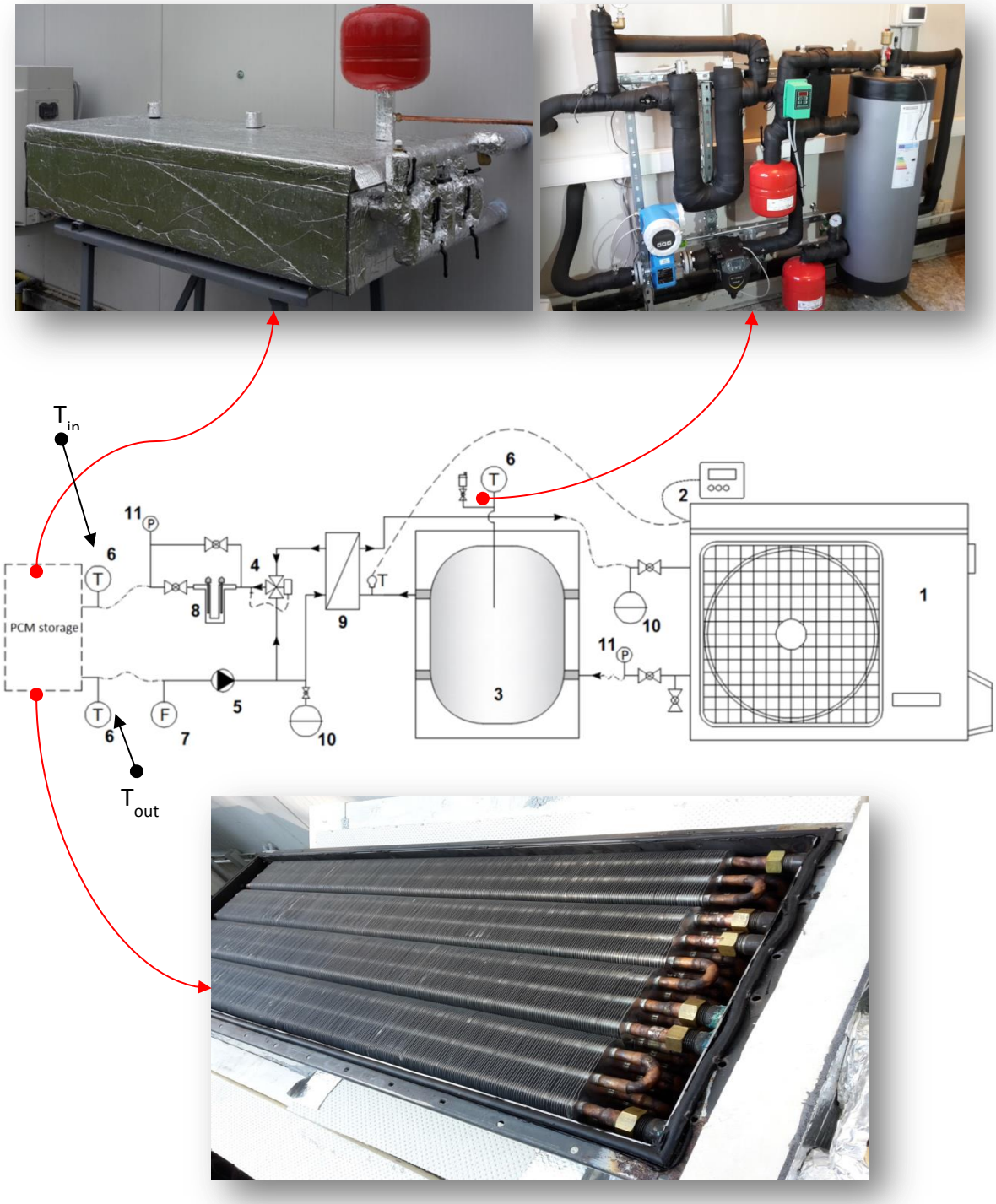


**Figure 1.** *The experimental setup; refer to Table 1 for details regarding the system components.*

The volume flow rate ($\dot{V}$, used to compute the mass flow rate $\dot{m}$) of the propylene-water-glycol mixture was measured by an electromagnetic flowmeter (component*#7* in Figure 1); the inlet ($T_{in}$) and outlet ($T_{out}$) temperatures of the *PCM* storage were measured by RTD Pt100 4wire 1/5DIN, inserted within the pipes (components*#6* in Figure 1). A RTD Pt100 4wire 1/5DIN temperature probe monitored the "*buffer storage tank*" temperature. All temperature probes were verified, prior to experimentation, with an in-house calibration by using a thermostatic bath. The power consumption of the systems was monitored by a multifunction electric meter. All data were recorded every 6 seconds (Advantech ADAM 5000 and 4000 data logging).

**Table 1.** *Details of the system components displayed in Figure 1.*

| Code name (Figure 1) | Equipment | Uncertainties |
|---|---|---|
| **1** | Reversible heat pump (MAXA, i-HWAK//V4 06, R410A) | -- |
| **2** | Remote control system for the reversible heat pump (provided with MAXA, i-HWAK//V4 06) | -- |
| **3** | Buffer storage tanks for heat pumps; 51l, water storage (*manufactured by Cordivari, product name: volano termico PdC50*) | -- |
| **4** | Deviation valve (*product name: comparato Nello Diamix Pro*) | -- |
| **5** | Variable speed circulation pump (*product name:* DEB Evolplus Small 60/180 M PWM, power: 5 ÷ 100 W) | -- |
| **6** | Temperature probe - RTD Pt100 (1/5DIN) | ±0,06 °C (0 °C) |
| **7** | Electromagnetic flow meter (*manufactured by* Endress & Hauser*, product name:* Promag DN15) | ±0,2% read value |
| **8** | Two electrical resistances (2x1500 W) | -- |
| **9** | Plate heat exchanger (*manufactured by Cordivari, product name: SLB20*) | -- |
| **10** | 8dm$^3$ expansion tank | -- |
| **11** | Pressure Transducer | ±0,5% read value |
| **Not shown in Figure 1** | Multifunction power and energy meter for electrical consumption measurement | ±0,2% read value |

## 2.2 The storage unit

As displayed in Figure 1, the *PCM* storage consists of a fin-and-tube heat exchanger surrounded by *PCM* material and placed in a tank (insulated by a 60 mm polystyrene layer and covered by a reflective material); in addition, the and-tube heat exchanger is connected with the hydraulic circuit of described in Section 2.1. Given the goals of this research as well as the outcome of Besagni et al. [10], the system is supposed to work within the range of 20 - 30 °C. Consequently, the commercial paraffin *RT26* (manufactured by *Rubitherm GmbH*, ref. [31]; see Table 2 for a list of its thermophysical properties), was selected after a screening of commercially available products (see the report of ref. [32]) and 58 kg of *PCM* were used to fill the volume available in the storage unit[3]. Based on the discussion proposed in

[3] Prior of testing PCM, water was tested as storage media and, in such case, 64 kg of water were used

the introduction, a fin-and-tube system has been selected, designed and built, modifying a commercial product (indeed, the view behind this research is to develop an economic viable technology). The present fin configuration has been selected, instead of longitudinal finds, following the outcomes of Medrano et al. [18]. Figure 1 and Figure 2 show the storage unit and a schematic drawing of the heat exchanger respectively.

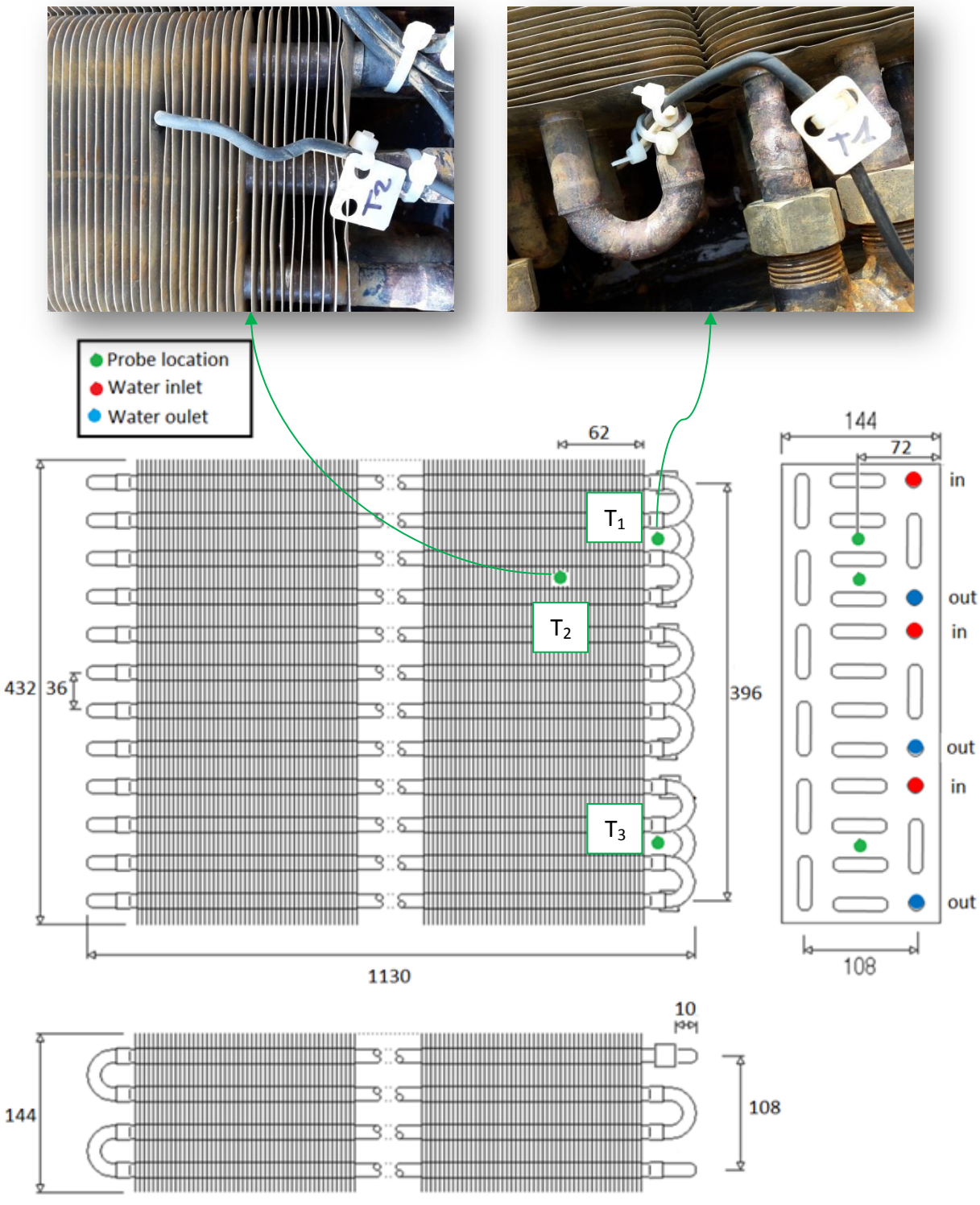


**Figure 2.** *Details of storage unit and RTD Pt100 temperature probe locations: measurements in [mm]*

The heat exchanger is connected to the test rig by an external manifold (Figure 1) and is composed by 12 copper tubes (14 mm inner diameter) and aluminum fins (thickness equal to 0.25 mm, pitch equal to 3 mm). Following the criteria discussed by Paloba et al. [22], such spacing is a compromise between easy *PCM* filling and high heat transfer capacity. To monitor the temperatures inside the storage unit, 3 RTD Pt100 (Class A, ±0,15 °C at 0 °C) were placed at different locations (see Figure 2). It is known that fin-and-tube *PCM* storage suffers from non-uniform heat exchange and phase change phenomena. To study the multi-scale effects of this issue, the hydraulic circuit of the heat exchanger was operated in both parallel and in the series configuration, by acting on the external manifold to modify the inlet conditions (Figure 3). The external tank is connected to a volume expansion vessel (10 l volume) and to an air safety valve; conversely, the hydraulic circuit is equipped with a safety valve.

**Table 2.** *Thermophysical properties of RT26* [31]

| Parameter | Value |
|---|---|
| **Melting/congealing temperature** | In the range of 25-26 °C (peak at 26 °C) |
| **Specific heat capacity** | 2 kJ/kg K |
| **Heat storage capacity** | 180 kJ/kg |
| **Liquid density** | 750 kg/m$^3$ |
| **Solid density** | 880 kg/ m$^3$ |
| **Heat conductivity** | 0.2 W/m K |

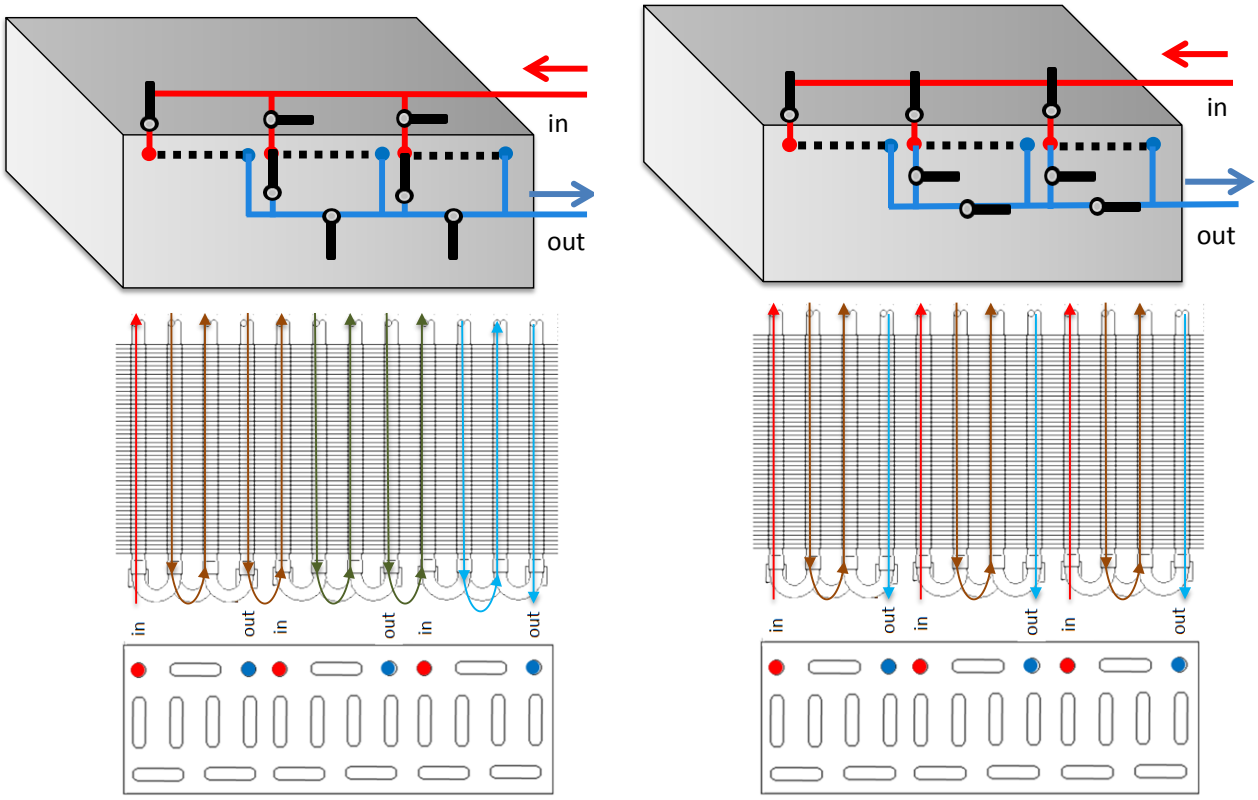


(a) series configuration (b) parallel configuration

**Figure 3.** *Details of series and parallel operation modes of the storage unit*

## 2.3 **Experimental procedure**

The experimental procedure has been designed to test the storage system under a real set of boundary conditions. The procedure is composed by a pre-conditioning phase (*phase#0*) and three main phases (*phases#1-3*):

*phase#0.* A pre-conditioning of the storage is obtained, by setting the storage unit at a constant and uniform temperature ($T_1$, $T_2$, $T_3$, $T_{in}$, $T_{out}$ are set at $T_{start}$ = 15 °C);

*phase#1.* The electrical resistances are switched on at constant power $P_{el}$ and the flow rate is circulated at volumetric flow rate equal to $\dot{V}_{heating}$;

*phase#2.* Charging is stopped (resistances are switched off) when $T_{average}$ (viz., the mean temperature within the storage unit, computed as the mean value between $T_1$, $T_2$ and $T_3$) is equal to $T_{heating}$. The flow rate is circulated till $T_{in}$, $T_{out}$, $T_1$, $T_2$ and $T_3$ reach the same temperature and keep it constant for 5 minutes;

*phase#3.* Valve (component*#4* in Figure 1) is opened to connect the storage unit with the "*buffer storage tank*" and the flow rate is circulated at $\dot{V}_{cooling}$ till $T_1$, $T_2$ and $T_3$ reach $T_{start}$ = 15 °C (heat pump is used to maintain the temperature of the buffer storage unit at 15 °C);

The procedure was applied to the cases listed in Table 3, to study the influence of prevailing boundary conditions (e.g., $P_{el}$ $T_{heating}$ and $\dot{V}$) on both the series and parallel configurations. In addition, water has been tested as storage media to clarify the influence of the material employed in the present storage unit.

**Table 3.** *Experimental matrix: details of the tested cases*

| Code name | Configuration | Test settings *(see Section 2.3 for further details regarding the procedure)* |
|---|---|---|
| **WATER** | Parallel | $P_{el} = 1.3kW, T_{heating} = 35°C\ \dot{V}_{heating} = 370m^3/h, \dot{V}_{cooling} = 430m^3/h$ |
| **PCM 1** | Parallel | $P_{el} = 1.3kW, T_{heating} = 35°C\ \dot{V}_{heating} = 370m^3/h, \dot{V}_{cooling} = 430m^3/h$ |
| **PCM 2** | Series | $P_{el} = 1.3kW, T_{heating} = 35°C, \dot{V}_{heating} = 370m^3/h, \dot{V}_{cooling} = 370m^3/h$ |
| **PCM 3** | Parallel | Compared with *PCM 1,* $P_{el} = 2.8kW$ |
| **PCM 4** | Series | Compared with *PCM 2,* $P_{el} = 2.8kW$ |
| **PCM 5** | Parallel | Compared with *PCM 1,* $T_{heating} = 40°C$ |
| **PCM 6** | Series | Compared with *PCM 2,* $T_{heating} = 40°C$ |
| **PCM 7** | Parallel | Compared with *PCM 1,* $T_{heating} = 50°C$ |
| **PCM 8** | Series | Compared with *PCM 2,* $T_{heating} = 50°C$ |
| **PCM 9** | Parallel | Compared with *PCM 1,* $P_{el} = 0.7kW$ |
| **PCM 10** | Series | Compared with *PCM 2,* $P_{el} = 0.7kK$ |
| **PCM 11** | Parallel | Compared with *PCM 1,* $P_{el} = 2.0kK$ |
| **PCM 12** | Series | Compared with *PCM 2,* $P_{el} = 2.2kK$ |
| **PCM 13** | Parallel | Compared with *PCM 1,* $\dot{V}$ is reduced : $\dot{V}_{heating} = 300m^3/h, \dot{V}_{cooling} = 300m^3/h$ |
| **PCM 14** | Series | Compared with *PCM 2,* $\dot{V}$ is reduced : $\dot{V}_{heating} = 190m^3/h, \dot{V}_{cooling} = 190m^3/h$ |
| **PCM 15** | Parallel | Compared with *PCM 1,* $\dot{V}$ is increased: $\dot{V}_{heating} = 540m^3/h, \dot{V}_{cooling} = 690m^3/h$ |

In the series mode, $\dot{V} = 370\, m^3/h$ is the maximum achievable flow rate owing to the higher pressure losses compared with the parallel configuration. In order to ensure the same cooling load in the cases "*PCM 2*" and "*PCM 1*" cases, $\dot{V}_{cooling}$ has been set equal to $430 m^3/h$ in the parallel configuration; the variations in the flow rate for cases *PCM 13-15* reflect this initial choice. All the experimental tests have been conducted in the same periods of the day, provided that the ambient conditions (*T*, relative humidity, solar radiation) were similar in value. The outdoor temperature and humidity were measured by a Pt100 4wire hygrometer (Siap + Micros); the solar irradiance was measured by a thermopile pyranometers (Kipp&Zonen CMP11). Repeatability tests were conducted prior to the experimentation (in both the parallel and series configurations).

## 2.4 System performance

Charge/discharge energy ($E_{th}$) towards/from the storage unit is computed as the integral of the instantaneous power ($\dot{Q}$) during the whole heat exchange process. $\dot{Q}$ (Eq. (1)) and $E_{th}$ (Eq. (2)) are computed based on the energy balance on the water-side, under the assumption of an adiabatic process[4]:

$$\dot{Q} = \dot{m} c_p (T_{in} - T_{out}) = \dot{V} \rho c_p (T_{in} - T_{out}) \quad (1)$$

$$E_{th} = \sum_{t=0}^{n=N} Q \quad (2)$$

where $t$ is the temporal variable, based on the time discretization of the measurements (6 seconds) Based on the instrumentation, it is estimated that $\dot{Q}$ is computed within the range of ± 0.03 kW of its value (expanded uncertainty). The uncertainty was calculated according to the ASME guidelines [33] on reporting uncertainties in experimental measurements based on the deviation in the experimental parameters.

Based on Eq. (2), the mass energy density ($\varepsilon_m$) and the volume energy density ($\varepsilon_V$) are computed as follows:

$$\varepsilon_m = \frac{E_{th}}{m_{PCM}} = f(x) = \begin{cases} \frac{E_{th}}{58kg} & PCM \\ \frac{E_{th}}{64kg} & water \end{cases} \quad (3)$$

[4] Heat losses were measured prior to the experimental study and have been found negligible, also taking into account the time scales of the heat transfer process.

$$\varepsilon_V = \frac{E_{th}}{V} = \frac{E_{th}}{64l} \quad (4)$$

To assess the performance of the heat exchanger on a lumped point of view, the parameter *UA* is computed following the proposal of Palomba et al. [22]:

$$UA = \frac{\dot{Q}}{\left(T_{average} - \frac{T_{in} - T_{out}}{2}\right)} \quad (5)$$

Where $T_{average}$ (viz., the mean temperature within the storage unit, computed as the mean value between $T_1$, $T_2$ and $T_3$

# 3 Experimental results

This section presents the global performance of the storage unit (Section 3.1) and the instantaneous values of the monitored variables (Section 3.2). In the forthcoming sections, the present observations are compared with the literature and, in particular, with Palomba et al. [22] owing to the "*pilot-scale*" concept, the similar design criteria and the similar heat exchanger design. Such comparison will help future researchers who will design and test fin-and-tube based *PCM* storage systems.

## 3.1 Global performances

Table 4 summarizes the outcomes of the experimental study in a global point of view (viz., energy stored during the charging phase, $E_{th,heating}$, and the resulting energy density, $\varepsilon_{m,heating}$ and $\varepsilon_{v,heating}$). In the following, the effect of the storage material (water or *PCM*) is presented and, subsequently, the effect of the boundary conditions is discussed. For the sake of completeness, in Table 4 Reynolds number in the charging phase is listed too.

The effect of the storage material is analyzed by comparing two cases, namely "*Water*" and "*PCM 1*". In these cases, the heat exchanger was operated in the parallel configuration, implementing the same charging profile and the same boundary conditions. It is observed that *PCM* is able to store 65 % higher thermal energy compared with water, ensuring 81.9 % higher mass energy density and 65 % higher volume energy density. To provide a quantitative outcome of this observation, the influence of higher thermal energy stored in the dual-source *SAHPs* is estimated based on the methodology described in ref. [10]. Assuming that the *PCM* storage replaces the water-source storage (see the system layout of ref. [10]), a certain share of the thermal energy previously supplied with the air–source-evaporator is now provided by the *PCM* storage. Implementing this assumption within above-referenced method, it is

198 estimated that the dual-source *SAHP* described in ref. [10] with the *PCM* storage, has 6% lower electrical
199 consumptions (on a seasonal average point of view).

200 **Table 4.** *Experimental results: global performances – Details of the different tests in Table 2.*

| Code name | Layout (Figure 3) | $E_{th,heating}$ [kWh] | $\varepsilon_{m,heating}$ [kWh/kg] | $\varepsilon_{V,heating}$ [kWh/m$^3$] | $Re_{heating}$* [-] | Corresponding Figure(s) |
|---|---|---|---|---|---|---|
| **WATER** | Parallel | 2.0735 | 0.03240 | 32.40 | 12253 | Figure 4<br>Figure 6 |
| **PCM 1** | Parallel | 3.4182 | 0.05894 | 53.41 | 12110 | Figure 4<br>Figure 6<br>Figure 7<br>Figure 9 |
| **PCM 2** | Series | 3.7076 | 0.05793 | 57.93 | 4106 | Figure 8<br>Figure 10 |
| **PCM 3** | Parallel | 3.5888 | 0.05608 | 56.08 | 12137 | Figure 9<br>Figure 11<br>Figure 13 |
| **PCM 4** | Series | 3.7357 | 0.06441 | 58.37 | 4113 | Figure 10<br>Figure 11<br>Figure 14 |
| **PCM 5** | Parallel | 3.6972 | 0.06375 | 57.77 | 12144 | Figure 11 |
| **PCM 6** | Series | 3.9980 | 0.06247 | 62.47 | 4112 | Figure 12 |
| **PCM 7** | Parallel | 4.7843 | 0.07475 | 74.75 | 12117 | Figure 11 |
| **PCM 8** | Series | 4.7343 | 0.08163 | 73.97 | 4159 | Figure 12 |
| **PCM 9** | Parallel | 4.2116 | 0.07261 | 65.81 | 12020 | Figure 9 |
| **PCM 10** | Series | 3.9237 | 0.06131 | 61.31 | 4082 | Figure 10 |
| **PCM 11** | Parallel | 4.0954 | 0.06399 | 63.99 | 12034 | Figure 9 |
| **PCM 12** | Series | 3.6749 | 0.06336 | 57.42 | 4103 | Figure 10 |
| **PCM 13** | Parallel | 3.9238 | 0.06765 | 61.31 | 10172 | Figure 13 |
| **PCM 14** | Series | 3.4839 | 0.05444 | 54.44 | 2093 | Figure 14 |
| **PCM 15** | Parallel | 4.0561 | 0.06338 | 63.38 | 17900 | Figure 13 |

201 **Reynolds number computed based on the averaged value of the flow rate in the charging phase.*

202 As stated above, the proposed unit stores 65 % higher thermal energy, compared with a volume-equivalent water
203 storage unit, which is an improvement compared with the 50 % reported by Palomba et al. [22]. The difference
204 between the present study and ref. [22] may be related to the different operating conditions (i.e., high temperature
205 operation in ref. [22], which implies higher heat losses through the surrounding). In future studies, an optimization of
206 the proposed system will be carried out to improve the obtained performance, by tackling the limitations in the heat
207 transfer as well as the presence phase change "*stagnant region*" (to be detected by local measurements and/or
208 numerical simulations). Figure 4 proposes a more detailed view of above-results by showing $E_{th}$ and *UA* instantaneous
209 profiles. It is observed that, in the "*Water*" case, *UA* is in the range of 600 W/K (in the heating mode) and 900 W/K (in
210 the cooling mode); conversely, in the "*PCM 1*" case, *UA* is in the range of 400-500 W/K (in the heating/cooling modes).

211 It is worth noting that *UA* in the cooling mode is fluctuation as the instantaneous power is fluctuating as well (in the
212 cooling mode a constant load is not imposed; indeed, the deviating valve is opened and the heat pump is used to
213 maintain the buffer unit at a constant temperature). It has not escaped our notice that *UA* values at the beginning of
214 the cooling mode are slightly higher compared with the heating mode values. To clarify this observation, *"PCM 2"* case
215 has been considered as well (this case is characterized by a constant flowrate for both the heating and cooling modes).
216 In this case, *UA* values are very similar in both the heating and cooling modes. This observation suggests that above
217 differences are caused by the changes in the heating/cooling flowrates, which affects the overall heat transfer
218 performance. Indeed, *UA* values, for a given surface area, are related to the local thermal resistances.

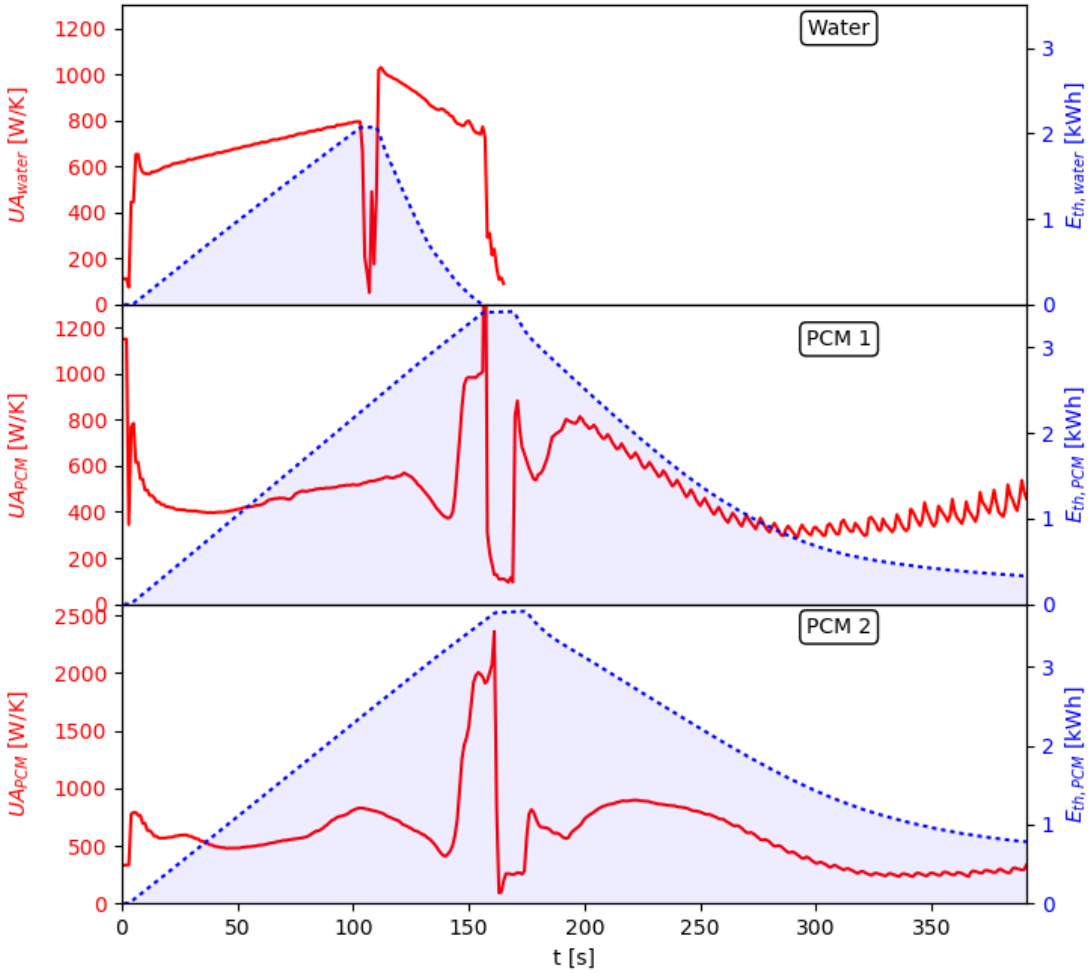


219
220 **Figure 4.** *Effect of the storage material on instantaneous profiles of $E_{th}$ and UA measurements: comparison between*
221 *"Water" (sensible storage) and "PCM 1-PCM 2" (latent/sensible storage) cases.*

222 The data presented in Figure 4 provide a rational basis to support the discussion regarding the limitations of the heat
223 transfer process, by pointing the cause towards the lower thermal conductivity of *PCM* compared with water (as

expected based on the previous literature [15]). In this perspective, it should be noted that, under the geometrical constrains of the system (viz., the small gap between the fins), the prevailing heat transfer mechanism is conduction (the onset of the convective motions is prevented). The observed range of *UA* values are higher compared with the ones reported by Palomba et al. [22] (approximately 100 W/K), supporting the correct design of the proposed storage. To complete the discussion proposed in Figure 4, Figure 5 compare $E_{th,heating}$ in different temperature intervals for "*Water*" (both the experimental values and the theoretical expectations) and "*PCM 1*" cases. The theoretical expectations are computed by using the water heat capacity, imposed temperature difference and the experimental recorded flow rates. Considering the water case, the theoretical value of $E_{th,heating}$ is lower compared with the experimental one, owing to the energy storage in the metallic parts. This statement is in agreement with the outcomes of ref. [22]. Comparing the "*Water*" and the "*PCM 1*" $E_{th,heating}$ values, it is observed that paraffin has higher storage capabilities in the "*phase change heat transfer*" region, rather than in the "*sensible heat transfer*" region (as expected). In conclusion, Figure 5 suggests that the present *PCM* has been correctly selected for the final application (viz., storage temperatures in the range of 20 - 30 °C).

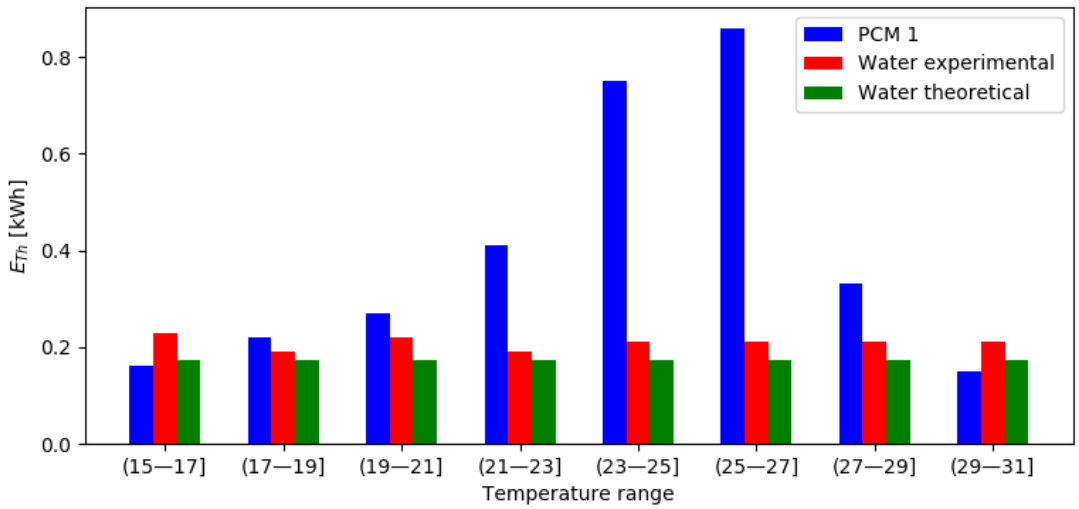


**Figure 5.** *Thermal energy stored ($E_{th}$) by the Water-CASE, the PCM-CASE#1 and the theoretical expectations of water (as defined by eq. (5)).*

Table 4 summarizes the effects of the boundary conditions on the global storage performance. Comparing the corresponding parallel/series cases, the stored energy is not highly influenced by the heat exchanger configuration (as displayed in Figure 5). However, changing between the series and the parallel configuration leads to other issues, as the different pressure losses in the hydraulic circuit (i.e., $\dot{V} = 370\ m^3/h$ is the highest flow rate that can be managed, given the present recirculation pump, in the series configuration). This concept is of practical relevance in large-scale

deployments of the proposed system; the parallel is more likely to be used in practical applications. Further studies should be conducted using the parallel configuration and the same flow rate as in the series configuration, but not major changes are expected. For the same system layout, the flow rate had an effect, as also described by Palomba et al. [22]. It is worth noting that Palomba et al. [22] operated the heat exchanger in the laminar, the transition and the turbulence flow regime; conversely, in our cases, we have not encompassed all the flow regimes and, in future studies, a more detailed analysis on the influence of the flow rates is needed. As expected, $T_{heating}$ has a relevant influence on $E_{th,heating}$, but its increasing should be limited for two reasons: (i) paraffin stability and (ii) *PCM* specific heat is lower compared with the one of water (see Figure 5).

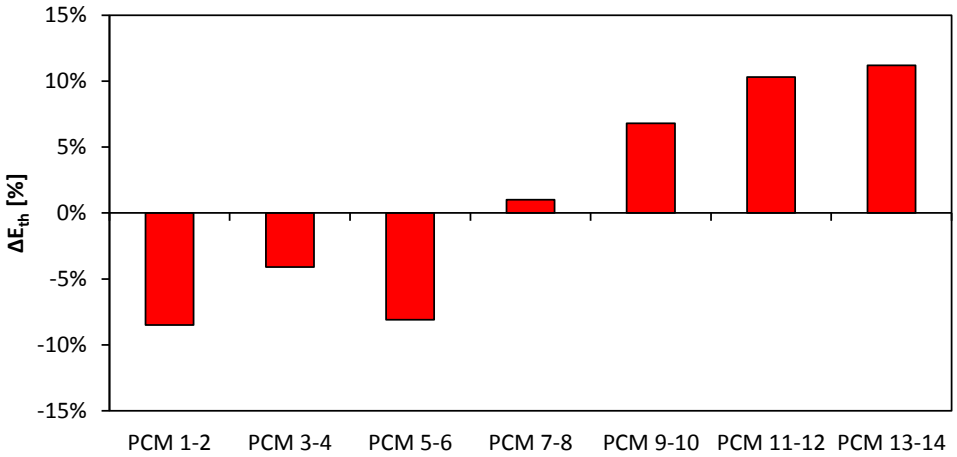


**Figure 6.** *Differences in $E_{th}$ values between corresponding cases (see Table 3 for further details on the case).*

## 3.2 Instantaneous performances

This section proposes a local description of the storage unit in terms of instantaneous values of the monitored variables. The global performances presented in Section 3.1 are the outcome of the local system parameters. In the following, first, the influence of the heat exchanger configuration (parallel/series) is discussed (Section 3.2.1) and, second, the effect of the different boundary conditions is discussed (Section 3.2.2).

### 3.2.1 Influence of the heat exchanger configuration

Figure 7 and Figure 8 compare two cases (namely, "*PCM 1*" parallel configuration and "*PCM 2*", series configuration), having the same value of $P_{el}$ and the same other boundary conditions. These figures show the instantaneous values of the inlet/outlet temperatures, internal temperatures, thermal power supplied/removed towards/from the storage units (Eq. (1)) and thermal energy stored (Eq. (2)).

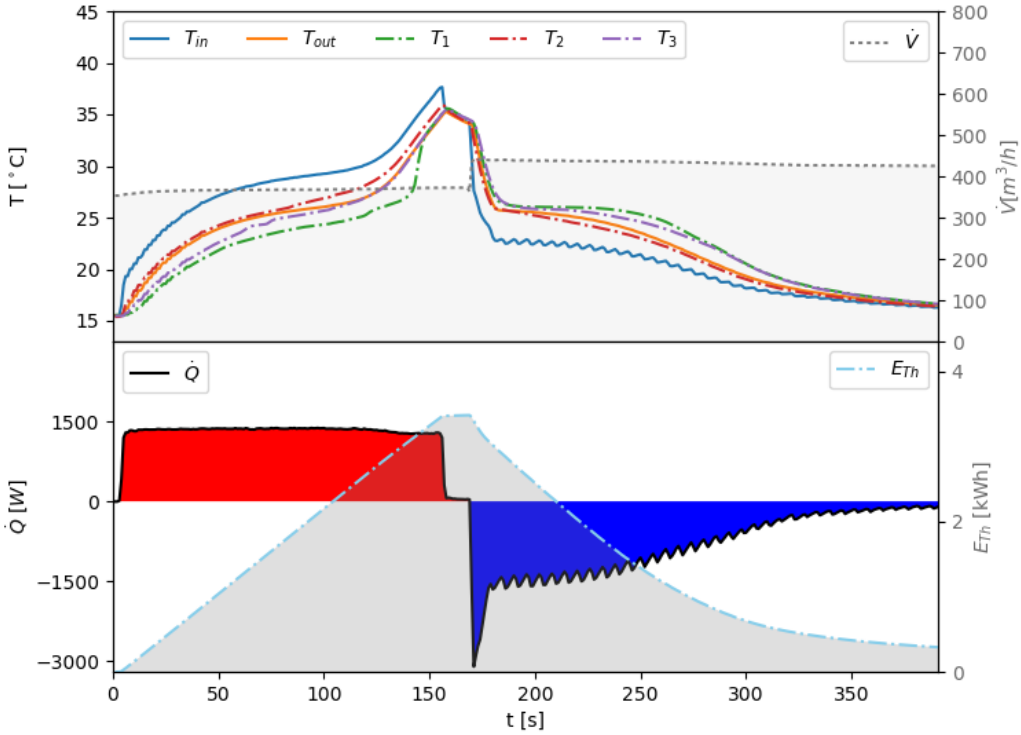


265 **Figure 7.** *Instantaneous profiles of temperatures (T), power supplied/removed ($\dot{Q}$) and thermal energy stored ($E_{th}$) –*

266 *Case PCM 1 (see Table 3 for further details on the case).*

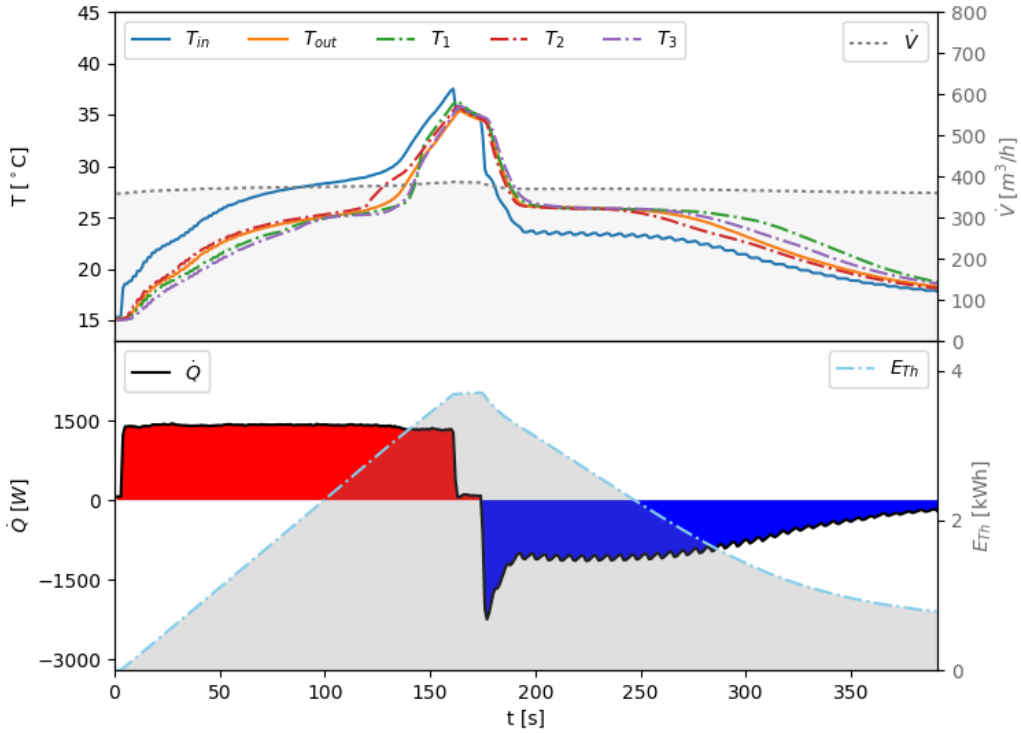


267

268 **Figure 8.** *Instantaneous profiles of temperatures (T), power supplied/removed ($\dot{Q}$) and thermal energy stored ($E_{th}$) –*

269 *Case PCM 2 (see Table 3 for further details on the case).*

Regardless of the heat exchanger configuration, all curves depict similar shapes. First, $T_{in}$ increases because of the thermal power supplied to the circulating water and, consequently, $T_{out}$ increases too. Subsequently $T_1$, $T_2$ and $T_3$ increase, owing to the thermal power supplied to the *PCM* by the heat exchanger. Looking closer at the shape of internal temperatures ($T_1$, $T_2$, $T_3$) six sub-phases are clearly identified (three in the heating mode and three in the cooling mode): (i) sensible heating (after the pre-conditioning phase, the whole *PCM* is in the solid phase); (ii) phase change (*PCM* is melting); (iii) sensible heating (*PCM* in the liquid phase); (iv) sensible cooling (*PCM* in the liquid phase), (v) phase change (solidification); (vi) sensible cooling (*PCM* is in the solid phase). After *PCM* sensible heating sub-phase, the *PCM* phase change is observed in the range of 25 – 26 °C (as expected) and, thus, the slope of internal temperatures reduce, as outcome of the phase change process. As expected and discussed in the previous literature [34, 35, 22] the range of phase change temperatures is hardly detectable, since the phase change process in *PCM* takes place in a broad range of temperatures. After melting is completed, sensible heating is observed again and the internal temperatures start increasing until $T_{heating}$ is reached and the charging is stopped. Subsequently, thermal energy is removed from the storage unit, by acting on the deviation valve (component#4 in Figure 1), and the internal temperatures decrease. The cooling phase is specular for the heating phase: after sensible heat exchange (*PCM* in the liquid phase), progressive *PCM* solidification is observed and, finally, sensible heat exchange (*PCM* in the solid phase) take place. It is worth noting that, within these phases, the internal temperatures are characterized by slow rise/decrease and, thus, the thermal energy supplied/removed towards/from the storage unit has a monotone increasing/decreasing trend. This observation is in agreement with the outcomes of ref. [22], where an explanation for this behavior was found in the characteristics of the heat exchange within the storage unit (viz., limited by the low *PCM* thermal conductivity), also verified in this case (Figure 4).

The influence of the heat exchanger configuration can be commented by taking into consideration the locations of the internal temperature probes (Figure 2): (i) probe#1 and probe#3 measure *PCM* temperature in a region with limited influence from the fins; (ii) probe#2 measures the temperature of the *PCM* material between two fins. During the charging phase of the parallel configuration (Figure 7), the difference between $T_3$ and $T_1$ increases with time; conversely, in the cooling phase, the duration of phase change at location #1 is longer compared with the other positions. These differences might be caused by a hydraulic maldistribution at the inlet of the heat exchanger. As expected, the central part of the heat exchanger (location #2 - closer to the tubes/fins) has higher melting rate and shows higher temperatures compared with the other probes. In the series configuration (Figure 8), the difference between the values of $T_1$ and $T_1$ is lower compared with the parallel configuration. On a global point of view, the

duration of the heating phase in both configurations is similar (which is caused by the fact that the charging phase is limited by the heating power of the testing rig), whereas the duration in the cooling mode in the series configuration is higher, possibly owing to the lower flow rate. The characteristics of the cooling phase in terms of temperatures (related to the PCM properties) and time-scales (viz., the duration of phase of change) make this storage suitable for an integration with the *SAHP* recently proposed by the authors [10]. The integration between the two technologies is very attractive and should be pursued in the forthcoming research activities.

### 3.2.2 Influence of the boundary conditions

This section discusses the relationships between the boundary conditions of the storage unit and the local/instantaneous variable profiles, to provide insights regarding the global performances listed in Table 4. To this end, Figures 9-14 display the instantaneous values of the measured variables, grouped as follows:

- influence of $P_{el}$ value in the parallel (Figure 9) and series (Figure 10) configurations;
- influence of $T_{heating}$ value in the parallel (Figure 11) and series (Figure 12) configurations;
- influence of $\dot{V}$ value in the parallel (Figure 13) and series (Figure 14) configurations.

Generally speaking, in all cases, and all the heat transfer sub-phases, previously discussed, are clearly recognizable and UA values are comparable between all different cases, thus suggesting that the local scale is characterized by limitation imposed by conductive phenomena.

First, the influence of the instantaneous thermal energy provided to the storage unit (related to $P_{el}$) is discussed. This parameter influences the time-scales and the phase change patterns within the storage unit. In general, $P_{el}$ value influences the dynamics of heat exchange by determining the evolution of the inlet temperature boundary conditions The lower is $P_{el}$, the more uniform is the heat transfer between the heat exchanger and the *PCM* material, as deduced by the profiles of internal temperature (Figure 9 and Figure 10) and *UA* profiles. Indeed, the lower is $P_{el}$, the more uniform are *UA* values within the whole duration of the tests. Conversely, the higher is $P_{el}$, the faster is the melting rate, the higher are the differences between the internal temperatures and less uniform *UA* profiles are observed. In the parallel configuration (Figure 9), when increasing $P_{el}$ from 1.3 kW toward 2.0 kW and 2.8 kW, $T_2$ exhibit higher value, compared with $T_1$ and $T_3$, during the whole duration of the test. This outcome suggests different heat exchanger dynamics and patterns in the internal regions compared with the side locations. Conversely, passing from $P_{el}$ = 1.3 kW toward $P_{el}$ = 2.0 kW, the system is characterized by lower time-scales and all the temperature profiles follow the same

paths, suggesting no prevailing pathways in heat exchanger between the heat exchanger and the whole *PCM* material. Instead, in the series configuration (Figure 10), passing from $P_{el}$ = 1.3 kW toward $P_{el}$ = 2.0 kW and $P_{el}$ = 2.8 kW, the profiles of $T_1$, $T_2$ and $T_3$ follow different paths depending on the instantaneous thermal energy provided to the storage unit, even if $T_2$ always exhibits higher values. This observation is related to the heat exchanger configuration displayed in Figure 3. Conversely, passing from $P_{el}$ = 1.3 kW toward $P_{el}$ = 2.0 kW, the system is characterized by lower time-scales (viz., It means that the system is able to complete the process with a certain/lower time constrain) and all the temperature profiles follow the same paths except for $T_1$, which is characterized by higher duration of the phase change process. In general, these observations suggest that lumped parameter model of PCM storage unit should take into account, a one-dimensional discretization of the domain. Finally, these results suggest that the designed storage unit may be applied in a quite broad range of operating conditions; in the case of *SAHPs*, it is suitable to store the thermal energy in different seasons and period of the day, without major limitation at higher loads.

Figure 11 and Figure 12 show the effect of $T_{heating}$ on the parallel and series configurations, respectively. In particular, three conditions are compared (all characterized by $P_{el}$ = 2.8 kW), with $T_{heating}$ equal to 35 °C, 40 °C and 50 °C. In both the parallel and in the series configurations, when increasing $T_{heating}$ the sensible heat contribution increases, without a significant influence on the cooling phase dynamics. It is worth noting that the shape of temperature in the sensible heating region (*PCM* in the liquid phase) is constantly rising, suggesting that the influence of thermal losses towards the environment is rather marginal, owing to the low-temperature range as well as the insulation of the storage unit.

As widely accepted, and as stated by Palomba et al. [22] there are two prevailing factor, for a given design configuration: the (local) difference of temperatures between the heat exchanger and the paraffin and the flow rate. In this view, Figure 13 and Figure 14 show the effect of $\dot{V}$ on the parallel and series configurations, respectively. It is worth noting that, in the series mode, $\dot{V} = 370\ m^3/h$ represents the maximum value reachable for the employed circulating pump. For all the observed cases, the cumulative energy curves do not increases faster when increasing the flow rates, which is in disagreement with Palomba et al. [22]. In the parallel configuration (Figure 13), when the flowrate increases, the differences between the sensible and the latent heat transfer regions (see $T_1$ and $T_2$ profiles) increase too. It is worth noting that the heat exchanger, in this case, is operated having $Re_{heating}$ in the fully developed turbulence flow regime ($Re_{heating}$ increases from 10000 till 17000 – see Table 4). Indeed, at $\dot{V} = 540\ m^3/h$, the phase change region in the range of 25 – 26 °c is clearly visible. This outcome suggests that increasing the flowrate increases the uniformity of the local heat transfer (in the fully developed turbulent flow regime). In the series configuration,

when increasing $Re_{heating}$ from 2000 to 4000 (comparison $\dot{V} = 190\ m^3/h$ with the $\dot{V} = 370\ m^3/h$ case), a high non-uniformity of the heat transfer process is noted. This observation is justified by the transition from the laminar to the turbulent flow regime. In addition, besides the change in the flow conditions, a reasonable explanation for these outcomes is given by Palomba et al. [22], suggesting that the local phenomena are limited by conduction.

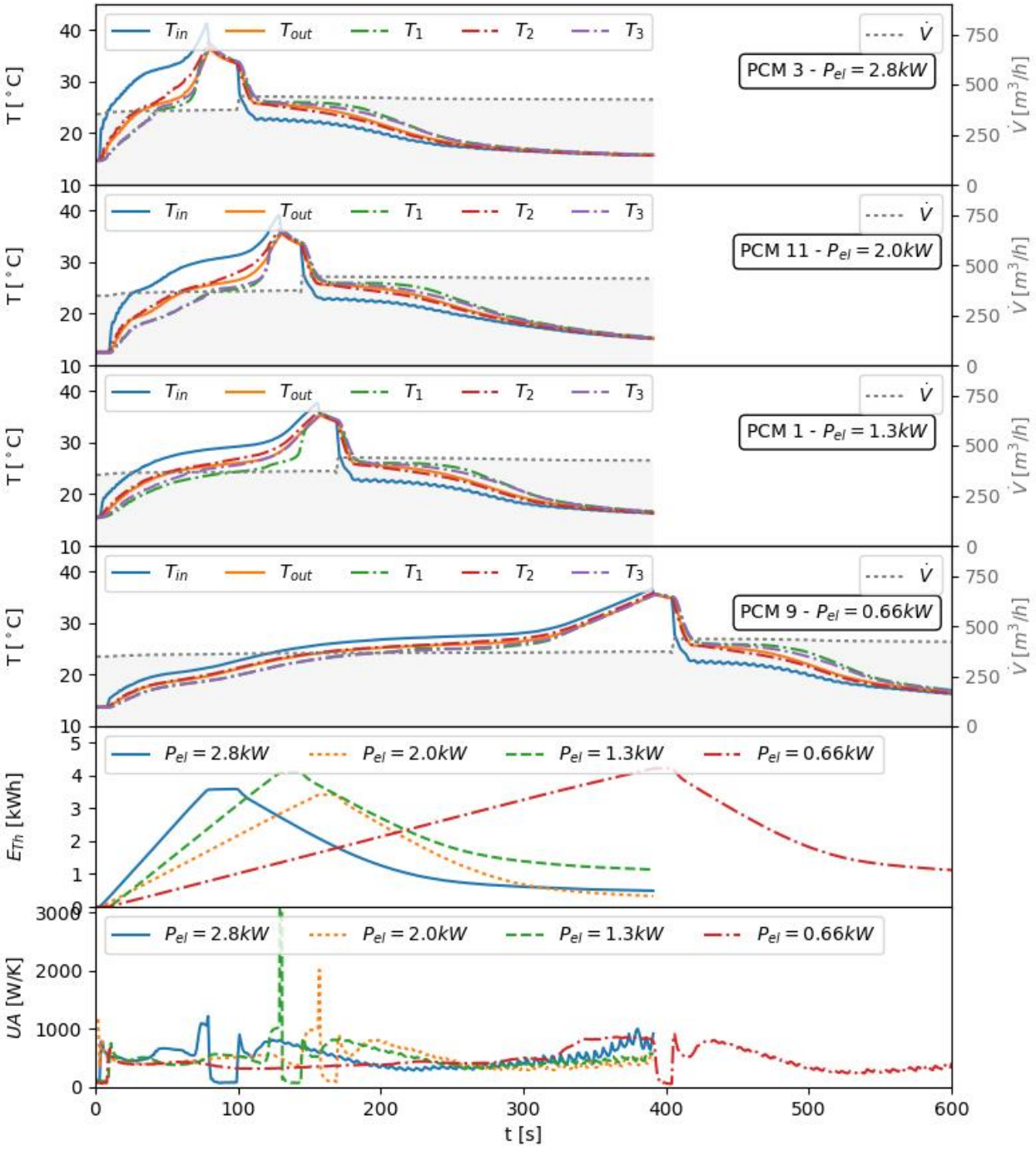


**Figure 9.** *Influence of $P_{el}$ on the instantaneous profiles of temperatures (T), power supplied/removed ($\dot{Q}$),* overall heat transfer coefficient (*UA*) *and thermal energy stored ($E_{th}$): parallel configuration – (see Table 3 for further details on the different cases).*

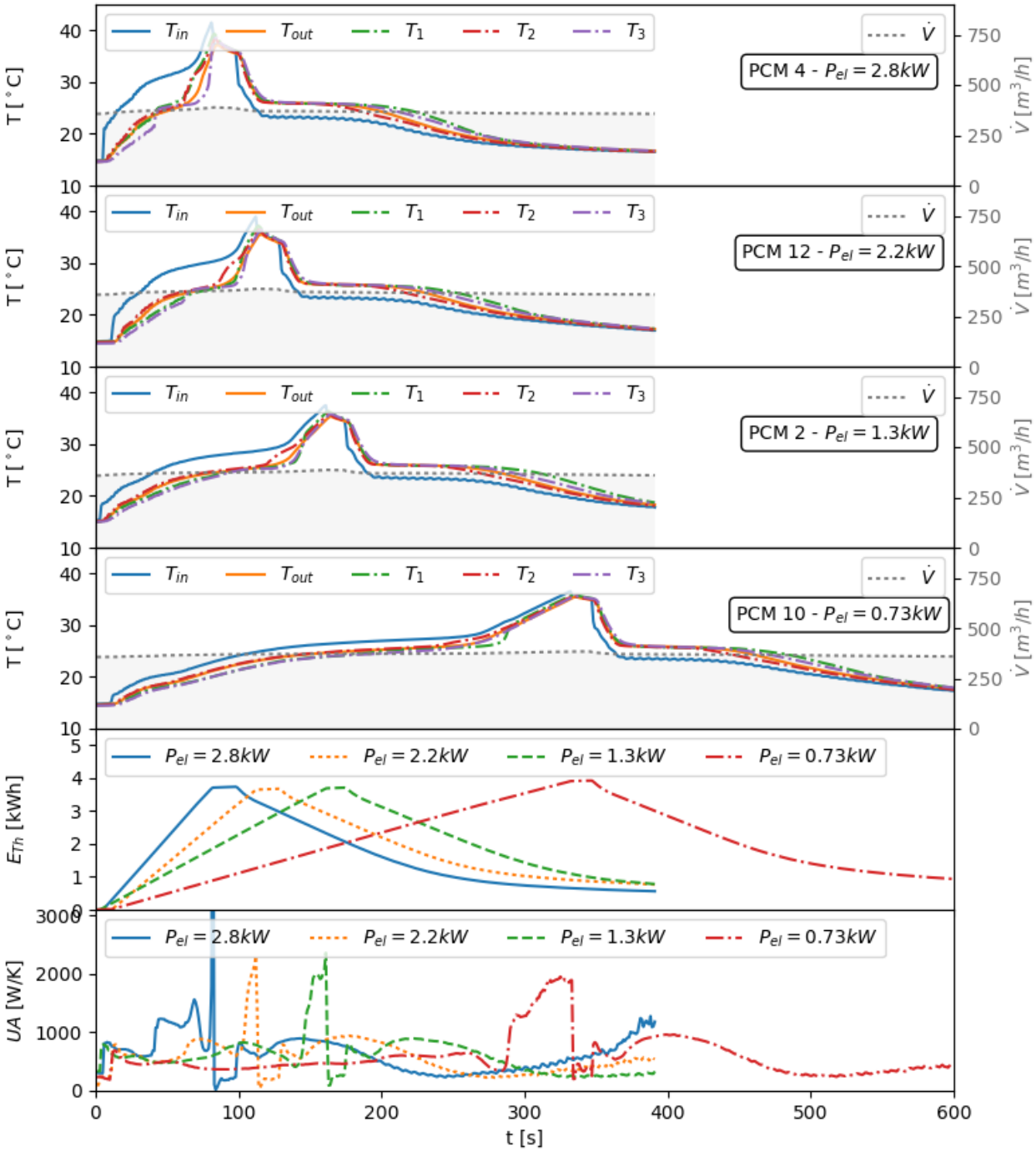


362

363 **Figure 10.** *Influence of $P_{el}$ on the instantaneous profiles of temperatures (T), power supplied/removed ($\dot{Q}$),* overall heat

364 transfer coefficient (*UA*) *and thermal energy stored ($E_{th}$): series configuration – (see Table 3 for further details on the*

365 *different cases).*

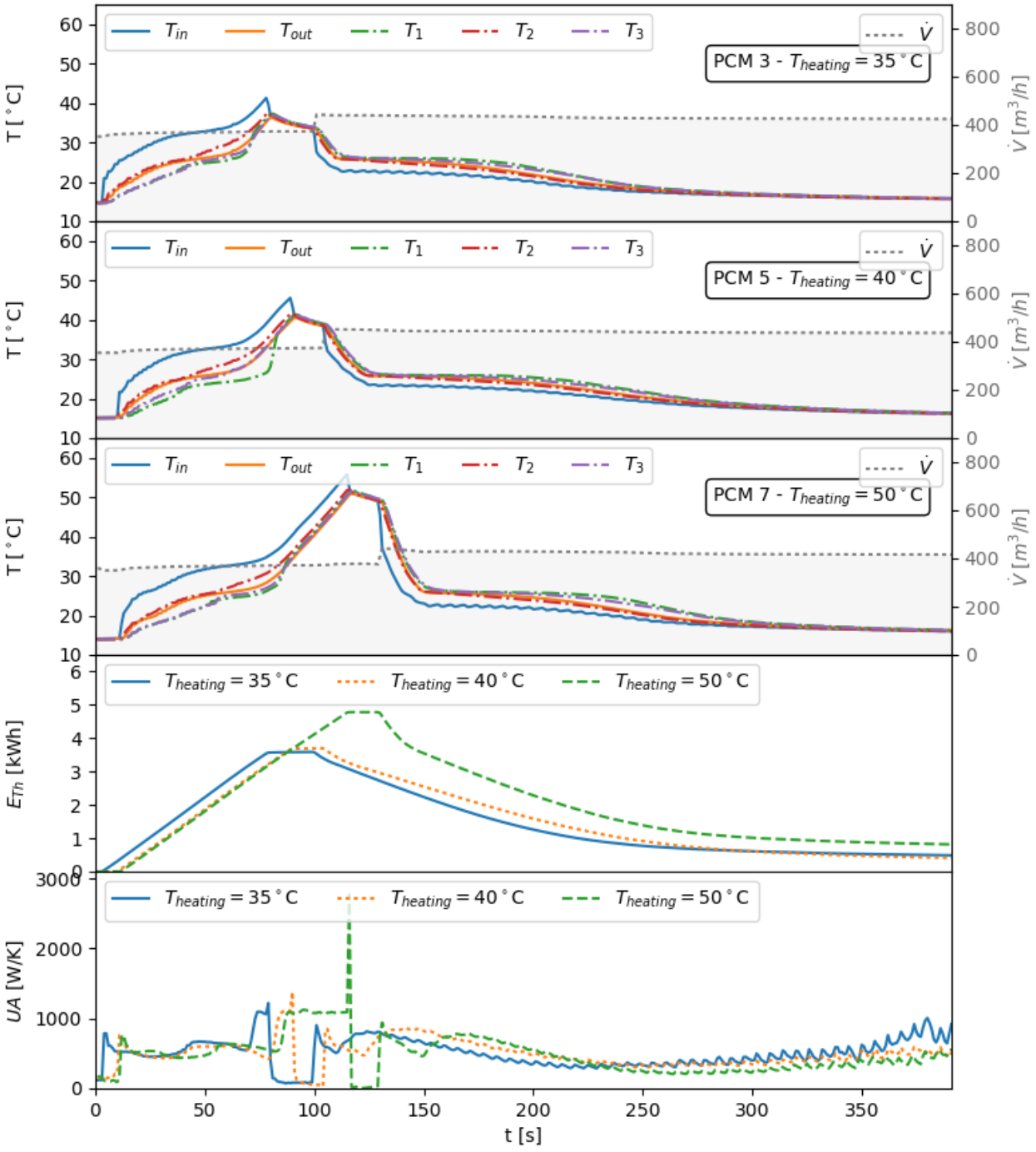


366

367 **Figure 11.** *Influence of $T_{heating}$ on the instantaneous profiles of temperatures (T), power supplied/removed ($\dot{Q}$),* overall

368 heat transfer coefficient (*UA*) *and thermal energy stored ($E_{th}$): parallel configuration – (see Table 3 for further details*

369 *on the different cases).*

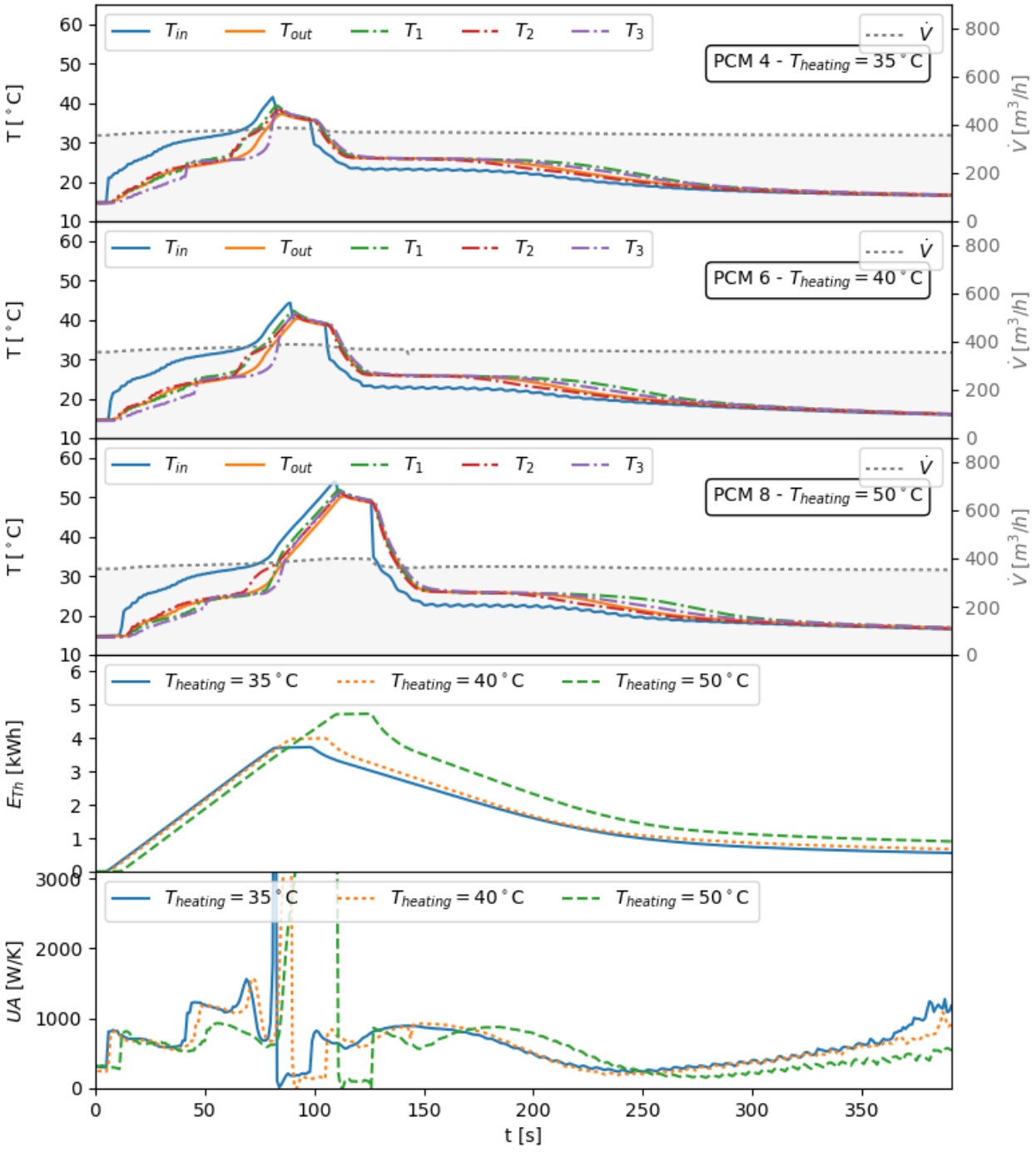


370

371 **Figure 12.** *Influence of $T_{heating}$ on the instantaneous profiles of temperatures (T), power supplied/removed ($\dot{Q}$),* overall

372 heat transfer coefficient (*UA*) *and thermal energy stored ($E_{th}$): series configuration – (see Table 3 for further details on*

373 *the different cases).*

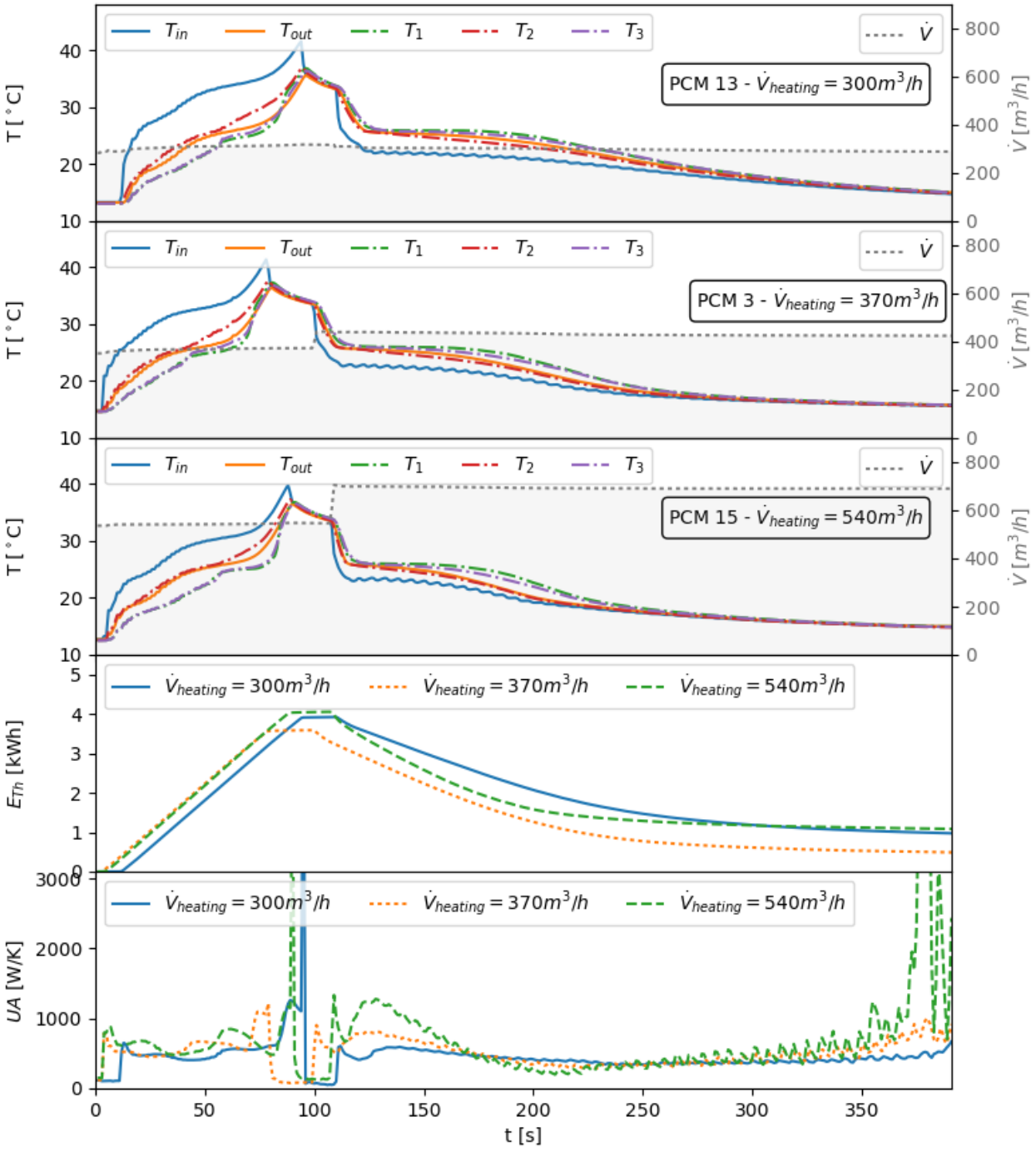


**Figure 13.** *Influence of $\dot{V}$ on the instantaneous profiles of temperatures (T), power supplied/removed ($\dot{Q}$),* overall heat transfer coefficient (*UA*) *and thermal energy stored ($E_{th}$): parallel configuration – (see Table 3 for further details on the different cases).*

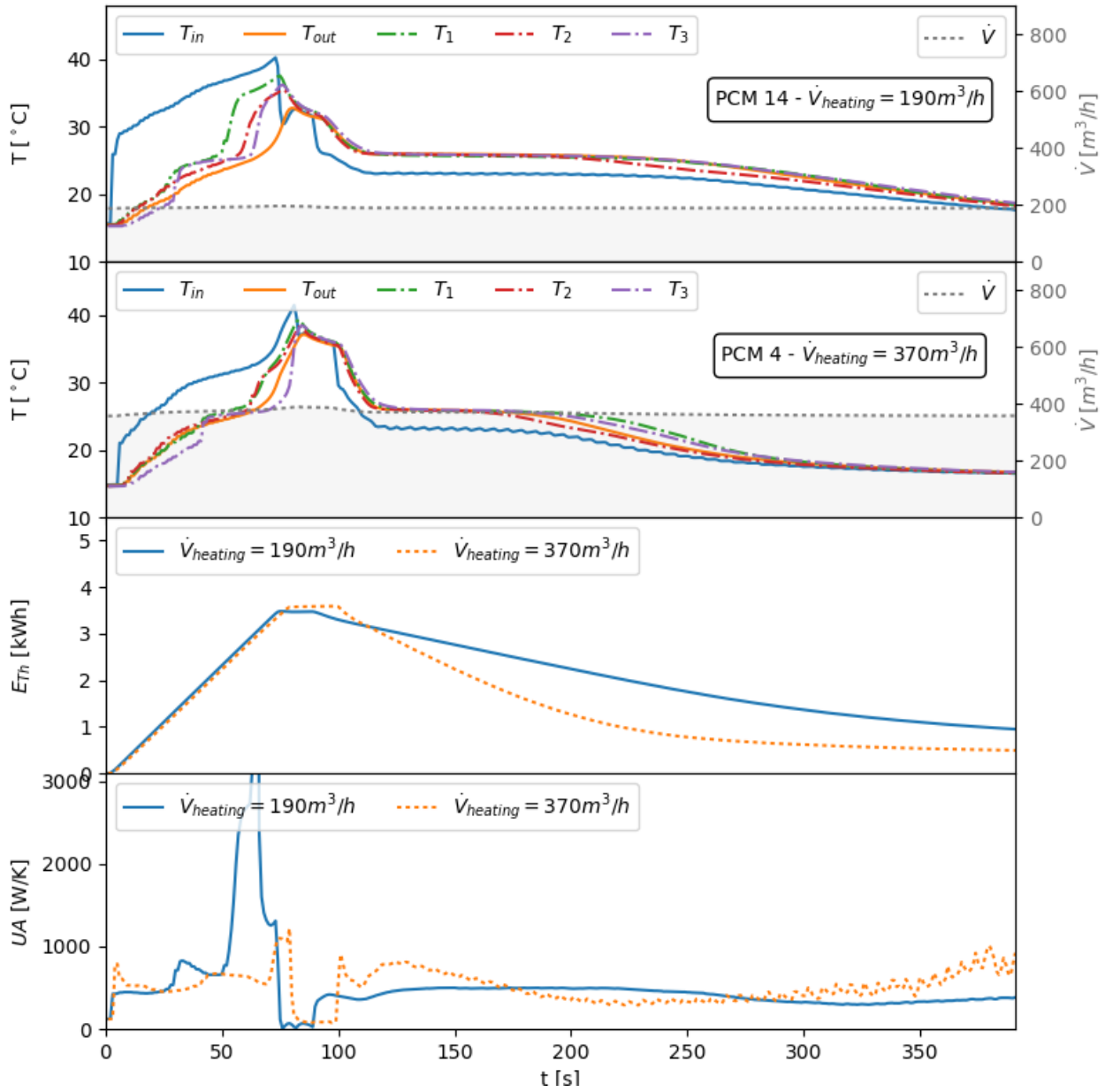


**Figure 14.** *Influence of $\dot{V}$ on the instantaneous profiles of temperatures (T), power supplied/removed ($\dot{Q}$),* overall heat transfer coefficient (*UA*) *and thermal energy stored ($E_{th}$): series configuration – (see Table 3 for further details on the different cases).*

# 4 Conclusions, outcomes and outlooks

This paper experimentally studied, in terms of global performances and local measurements, a pilot-scale fin-and-tube *PCM* storage, under a broad range of boundary conditions in different system configurations. Compared with a water-based storage unit, under the same boundary conditions, the proposed system stores 65 % higher thermal energy. On one hand, the parallel and series configuration showed similar results on a global point of view (viz., in term of the thermal energy storage in the charging phase), but with different local "*heat transfer patterns*". On the other hand, the series configuration is characterized by higher pressure losses, which should be carefully considered in large-scale deployments. The analysis of the instantaneous variable profiles demonstrated that the time-scales in the heating and cooling phases, under the different boundary conditions, are suitable for integration with the previously proposed *SAHP* [10]. In addition, the obtained dataset is attractive to validate numerical codes of *PCM*-based storage units. Future studies will be devoted to couple the proposed storage unit with the previously proposed *SAHP* as well as to improve the system design, to further tackle the low thermal conductivity issue.

# Acknowledgements

This work has been financed by the Research Fund for the Italian Electrical System in compliance with the Decree of Minister of Economic Development April 16, 2018.

# References

[1] D. Brounen, N. Kok and J. M. Quigley, «Residential energy use and conservation: Economics and demographics,» *European Economic Review,* vol. 56, pp. 931-945, 2012.

[2] *An EU Strategy on Heating and Cooling, COM(2016) 51 Final; European Commission: Brussels, Belgium, 2016,* 2016.

[3] EUROSTAT, «Energy consumption in households 2017,» EUROSTAT, 2017.

[4] G. Besagni and M. Borgarello, «The determinants of residential energy expenditure in Italy,» *Energy,* vol. 165, pp. 369-386, 2018.

[5] E. M. Craparo and J. G. Sprague, «Integrated supply- and demand-side energy management for expeditionary environmental control,» *Applied Energy,* Vol. %1 di %2233-234, pp. 352-366, 2019.

[6] A. Arteconi, N. J. Hewitt and F. Polonara, «Domestic demand-side management (DSM): Role of heat pumps and thermal energy storage (TES) systems,» *Applied Thermal Engineering,* vol. 51, pp. 155-165, 2013.

[7] J. Allison, K. Bell, J. Clarke, A. Cowie, A. Elsayed, G. Flett, G. Oluleye, A. Hawkes, G. Hawker, N. Kelly, M. M. M. de Castro, T. Sharpe, A. Shea, P. Strachan and P. Tuohy, «Assessing domestic heat storage requirements for energy flexibility over varying timescales,» *Applied Thermal Engineering,* vol. 136, pp. 602-616, 2018.

[8] D. N. Nkwetta, P.-E. Vouillamoz, F. Haghighat, M. El-Mankibi, A. Moreau and A. Daoud, «Impact of phase change materials types and positioning on hot water tank thermal performance: Using measured water demand profile,» *Applied Thermal Engineering,* vol. 67, pp. 460-468, 2014.

[9] M. Buker and S. B. Riffat, «Solar assisted heat pump systems for low temperature water heating applications: A systematic review,» *Renewable and Sustainable Energy Reviews,* vol. 55, pp. 399-413, 2016.

[10] G. Besagni, L. Croci, R. Nesa and L. Molinaroli, «Field study of a novel solar-assisted dual-source multifunctional heat pump,» *Renewable Energy,* vol. 132, pp. 1185-1215, 2019.

[11] H. Zhang, J. Baeyens, G. Cáceres, J. Degrève e Y. Lv, «Thermal energy storage: Recent developments and practical aspects,» *Progress in Energy and Combustion Science,* vol. 53, pp. 1-40, 2016.

[12] S. Y. Kee, Y. Munusamy and K. S. Ong, «Review of solar water heaters incorporating solid-liquid organic phase change materials as thermal storage,» *Applied Thermal Engineering,* vol. 131, pp. 455-471, 2018.

[13] M. Mohanraj, Y. Belyayev, S. Jayaraj and A. Kaltayev, «Research and developments on solar assisted compression heat pump systems – A comprehensive review (Part A: Modeling and modifications),» *Renewable and Sustainable Energy Reviews,* pp. -, 2017.

[14] H. Mehling and L. F. Cabeza, Heat and cold storage with PCM - An up to date introduction into basics and applications, Springer-Verlag Berlin Heidelberg, 2008.

[15] M. M. Kenisarin, «Thermophysical properties of some organic phase change materials for latent heat storage. A

review,» *Solar Energy,* vol. 107, pp. 553-575, 2014.

[16] J. P. da Cunha and P. Eames, «Thermal energy storage for low and medium temperature applications using phase change materials – A review,» *Applied Energy,* vol. 177, pp. 227-238, 2016.

[17] J. P. da Cunha and P. Eames, «Compact latent heat storage decarbonisation potential for domestic hot water and space heating applications in the UK,» *Applied Thermal Engineering,* vol. 134, pp. 396-406, 2018.

[18] M. Medrano, M. O. Yilmaz, M. Nogués, I. Martorell, J. Roca and L. F. Cabeza, «Experimental evaluation of commercial heat exchangers for use as PCM thermal storage systems,» *Applied Energy,* vol. 86, pp. 2047-2055, 2009.

[19] F. Agyenim, P. Eames and M. Smyth, «A comparison of heat transfer enhancement in a medium temperature thermal energy storage heat exchanger using fins,» *Solar Energy,* vol. 83, pp. 1509-1520, 2009.

[20] H. Eslamnezhad and A. B. Rahimi, «Enhance heat transfer for phase-change materials in triplex tube heat exchanger with selected arrangements of fins,» *Applied Thermal Engineering,* vol. 113, pp. 813-821, 2017.

[21] A. Acır and M. E. Canlı, «Investigation of fin application effects on melting time in a latent thermal energy storage system with phase change material (PCM),» *Applied Thermal Engineering,* vol. 144, pp. 1071-1080, 2018.

[22] V. Palomba, V. Brancato and A. Frazzica, «Experimental investigation of a latent heat storage for solar cooling applications,» *Applied Energy,* vol. 199, pp. 347-358, 2017.

[23] P. Dolado, A. Lazaro, J. M. Marin and B. Zalba, «Characterization of melting and solidification in a real-scale PCM–air heat exchanger: Experimental results and empirical model,» *Renewable Energy,* vol. 36, pp. 2906-2917, 2011.

[24] G. Peiró, J. Gasia, L. Miró and L. F. Cabeza, «Experimental evaluation at pilot plant scale of multiple PCMs (cascaded) vs. single PCM configuration for thermal energy storage,» *Renewable Energy,* vol. 83, pp. 729-736, 2015.

[25] G. Zsembinszki, P. Moreno, C. Solé, A. Castell and L. F. Cabeza, «Numerical model evaluation of a PCM cold storage tank and uncertainty analysis of the parameters,» *Applied Thermal Engineering,* vol. 67, pp. 16-23, 2014.

[26] M. Kabbara, D. Groulx and A. Joseph, «A parametric experimental investigation of the heat transfer in a coil-in-

tank latent heat energy storage system,» *International Journal of Thermal Sciences,* vol. 130, pp. 395-405, 2018.

[27] J. Gasia, J. M. Maldonado, F. Galati, M. D. Simone and L. F. Cabeza, «Experimental evaluation of the use of fins and metal wool as heat transfer enhancement techniques in a latent heat thermal energy storage system,» *Energy Conversion and Management,* vol. 184, pp. 530-538, 2019.

[28] A. Frazzica, M. Manzan, A. Sapienza, A. Freni, G. Toniato and G. Restuccia, «Experimental testing of a hybrid sensible-latent heat storage system for domestic hot water applications,» *Applied Energy,* vol. 183, pp. 1157-1167, 2016.

[29] A. Frazzica, Recent Advancements in Materials and Systems for Thermal Energy Storage, Springer, 2018.

[30] A. Frazzica, V. Palomba, D. L. Rosa and V. Brancato, «Experimental comparison of two heat exchanger concepts for latent heat storage applications,» *Energy Procedia,* vol. 135, pp. 183-192, 2017.

[31] Rubitherm GmbH, «RT 26,» [Online]. Available: www.rubitherm.eu/en/index.php/productcategory/organische-pcm-rt. [06 02 2019].

[32] Besagni, Giorgio; Croci, Lorenzo; Viani, Silvano and Nesa, Riccardo, «Architetture innovative per la climatizzazione: descrizione e risultati dell'attività,» Ricerca di sistema, RSE, n, 18001222, Milan, 2017.

[33] R. B. Abernethy, R. P. Benedict and R. B. Dowdell, «ASME Measurement Uncertainty,» *ASME. J. Fluids Eng.,* vol. 107(2), pp. 161-164, 1985.

[34] K. Cho and S. H. Choi, «Thermal characteristics of paraffin in a spherical capsule during freezing and melting processes,» *International Journal of Heat and Mass Transfer,* vol. 43, pp. 3183-3196, 2000.

[35] B. Torregrosa-Jaime, A. López-Navarro, J. M. Corberán, J. C. Esteban-Matías, L. Klinkner and J. Payá, «Experimental analysis of a paraffin-based cold storage tank,» *International Journal of Refrigeration,* vol. 36, pp. 1632-1640, 2013.

400

401